

The Influence of V-Defects, Leakage, and Random Alloy Fluctuations on the Carrier Transport in Red InGaN MQW LEDs

Huai-Chin Huang¹, Shih-Min Chen¹, Claude Weisbuch³, James S. Speck², and Yuh-Renn Wu^{1*}

¹*Graduate Institute of Photonics and Optoelectronics and Department of Electrical Engineering, National Taiwan University, Taipei 10617, Taiwan*

²*Materials Department, University of California, Santa Barbara, California 93106, USA*

³*Laboratoire de Physique de la Matière Condensée, CNRS, Ecole polytechnique, Institut Polytechnique de Paris, 91120 Palaiseau, France*

(*Author to whom correspondence should be addressed: yrwu@ntu.edu.tw)

(Dated: 3 February 2025)

Red InGaN-based light-emitting diodes (LEDs) exhibit lower internal quantum efficiencies (IQEs) than violet, blue, and green InGaN LEDs due to a reduction in radiative recombination rates relative to non-radiative recombination rates as the indium composition increases. Additionally, the larger polarization and band offset barriers between high indium content InGaN quantum wells and GaN quantum barriers increase the forward voltage. In blue and green LEDs, random alloy fluctuations and V-defects play a key role in reducing the forward voltage. When V-defects are present, either naturally or intentionally introduced, they create an alternative path for carrier injection into the MQWs through the V-defect sidewalls. This injection mechanism explains the turn-on voltages of green LEDs. However, in InGaN red LEDs, these two phenomena do not reduce the forward voltage as effectively as in blue and green LEDs, and consequently, the computed forward voltage remains significantly higher than the measured one. Furthermore, currents are observed at low voltages before the turn-on voltage ($V < \hbar\omega/e = 2.0\text{V}$) of red LEDs. To address this, we introduce dislocation-induced tail states in the modeling, suggesting that leakage current through these states may play a significant role both below and at turn-on voltages. The simulation also indicates that leakage carriers below turn-on accumulate, partially diffuse in the QWs, screen the polarization-induced barrier in the low injection regime, and further reduce the forward voltage. Despite these beneficial effects, a drawback of dislocation-induced tail states is the enhanced nonradiative recombination in the dislocation line region. This study provides a detailed analysis of device injection physics in InGaN QW red LEDs and outlines potential optimization strategies.

Keywords: red nitride-based μ -LEDs; V-defect; random alloy fluctuation; tail states

I. INTRODUCTION

In recent years, the study of indium gallium nitride (InGaN) materials has gained significant attention for their applications in micro light-emitting diodes (μ -LEDs). The superior efficiency, thermal stability, and emission characteristics of InGaN-based red-green-blue (RGB) micro-LEDs have made them increasingly desirable, especially as display technologies trend toward smaller chip and pixel sizes¹⁻⁴.

Regarding efficiency, blue InGaN LEDs achieve peak internal quantum efficiency (IQE) exceeding 90% at a current density of 1-10 A/cm²⁴⁻⁶. However, improving the IQE of red InGaN LEDs has proven particularly challenging, primarily due to the “green gap” with the factors contributing to the green gap being even more pronounced in the red spectral region^{7,8}. A key reason for the lower efficiency of high-indium-content InGaN QWs is the longer radiative lifetime caused by the large polarization-induced electric field in the QWs, which results in reduced electron-hole overlap⁹ relative to other non-radiative recombination mechanisms. Another challenge is the lower crystal quality of the QWs due to the relatively low growth temperature required for high-indium-content InGaN QWs. Additionally, the wall-plug efficiency (WPE) is affected by the operating voltage, which is primarily increased due to vertical carrier injection being significantly hindered by the large polarization-induced energy barriers at the quantum well/quantum barrier interfaces and the

large band offsets⁹⁻¹². However, experimental results show that the turn-on voltage of red LEDs is close to its theoretical value, indicating the presence of alternative carrier injection mechanisms beyond vertical injection.

Two mechanisms that reduce the turn-on voltage in blue and green LEDs have been previously identified and simulated. The natural alloy fluctuation of the InGaN QW material provides local reductions in the barriers for vertical transport in GaN-based blue LEDs (QBs) (Figs. 1(c) and 1(d))^{13,14}, enabling percolative paths for currents at lower applied voltages than those required in uniform materials. However, natural alloy disorder alone is insufficient to significantly reduce the barriers for vertical transport in green or red LEDs, leading to their higher forward voltage. One approach to mitigating this issue is carrier injection through V-defects, which are three-dimensional features that form under kinetically limited epitaxial growth conditions (Figs. 1(a) and 1(b))^{13,15-25}. Simulations of carrier injection through the shallower and semipolar MQWs of the V-defect sidewalls show that substantial lateral hole injection into the quantum wells occurs at lower forward voltages than for vertical injection, complementing the vertical injection path. Thus, V-defects enhance the LED WPE by reducing the forward voltage^{10,26,27}. However, their presence may also reduce the IQE due to the non-radiative dislocation region of the V-defect²⁷. In green LEDs, V-defects ultimately improve WPE, as the voltage reduction outweighs the potential decrease in IQE. With sidewall injection from V-defects

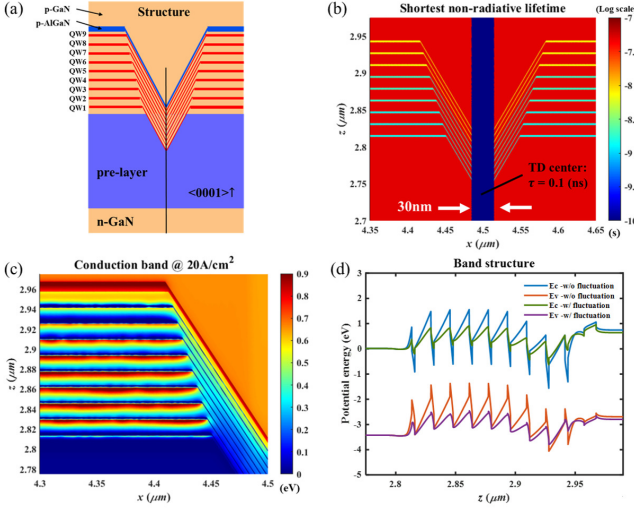


FIG. 1. (a) Structure of red LED from Ref [8]. (b) Cross-section of a V-defect and threading dislocation line at the of the V-defect. The TD dislocation line is modeled as a 30 nm diameter cylinder with a high density of fast nonradiative traps, and a short nonradiative lifetime value in this region. (c) Conduction band potential plotted in log scale. The strong polarization-related and band offset barriers for the c-plane QWs result in carriers flowing through semipolar planes with much-reduced energy variations. (d) Computed band extrema across the vertical LED structure away from the V-defect, taking alloy fluctuations into account (green and violet) or not (blue and red) curves, respectively. In the case of alloy fluctuations, band potential is spatially-averaged over the QW in-plane area. Random fluctuations aid carrier flow by decreasing the effective potential of quantum barriers²⁸.

in green LEDs, current flow becomes lateral in the quantum well, where limited lateral carrier diffusion leads to local current crowding near V-defects and minimal or no improvement in current efficiency droop.

However, in InGaIn red LEDs, simulations show that these two phenomena do not reduce the forward voltage to the same extent as in blue and green LEDs. Consequently, the computed forward voltage remains significantly higher than the measured one. Additionally, large leakage currents are observed at low voltages before the turn-on voltage ($V < \hbar\omega/e = 2.0\text{V}$) of red LEDs^{29,30}. To address this, we introduce dislocation-induced tail states in the modeling, as leakage current through such states may play a significant role both below and at turn-on voltages. The simulation further reveals that leakage carriers below turn-on accumulate in the QWs, screen the piezoelectric field-induced barrier in the low injection regime, and further lower the forward voltage. While this effect is beneficial, a drawback of these dislocation-induced tail states is the enhanced nonradiative recombination in the dislocation line region. Our model incorporates tail states in a two-dimensional drift-diffusion charge control (2D-DDCC) simulation, where we successively analyze the effects of: (1) random alloy fluctuations, (2) V-defects, and (3) tail states³¹ on device performance. Computational results indicate that: (1) alloy fluctuations promote radiative and Auger-Meitner re-

combination due to increased local carrier densities, with the Auger rate increasing more than the radiative rate, leading to a decrease in IQE; (2) V-defects reduce the turn-on voltage by enabling carrier transport across the lower In-content, semipolar sidewall QWs; and (3) carrier transport through tail states near dislocation lines and V-defects provides a better fit to experimental J-V curves at low biases ($V < \hbar\omega/e = 2.0\text{V}$)^{5,32} and results in a lower turn-on voltage³³.

In this paper, we systematically investigate the impact of V-defects, random alloy fluctuations, and tail states on red InGaIn μ -LEDs. The influence of carrier injection and the reduction of V_{for} will be examined at a current density of 20 A/cm^2 . This comprehensive study aims to enhance the understanding of these mechanisms and guide the development of reliable, high-efficiency red InGaIn μ -LEDs suited for next-generation display technologies.

II. METHODOLOGY

For this research, we employed an in-house two-dimensional drift-diffusion charge-control (2D-DDCC) solver to model carrier transport and the electrical properties of μ -LEDs (Fig. 2)³⁴. This solver is particularly well-suited for analyzing V-defects and random alloy fluctuations, both of which are crucial for understanding device behavior. First, the Poisson equation (1) was used to calculate the electrostatic potential (ψ) based on the charge distribution. Charge sources include free electrons (n) and holes (p), as well as ionized acceptors and donors, N_A^- and N_D^+ , respectively, while ρ_{pol} accounts for the polarization charge density, which depends on the local indium composition. Furthermore, the solver integrates the Localization Landscape (LL) theory^{28,35,36}, an advanced method that accounts for both quantum confinement effects and alloy disorder in determining the effective quantum potential $\frac{1}{\tau_{e,h}}$. This is achieved by substituting (2) for the conventional Schrödinger equation³⁵. The model integrates in the energy space using the Fermi-Dirac distribution (f_n, f_p) and the local density of states for electrons (N_c) and holes (N_v) in Eqs. (3) and (4) to compute carrier concentrations, where E_{fn} and E_{fp} denote the quasi-Fermi levels for electrons and holes, respectively.

$$\nabla \cdot (\epsilon \nabla \psi) = q(n - p + N_A^- - N_D^+ \pm \rho_{\text{pol}}) \quad (1)$$

$$\left(\frac{\hbar^2}{2m_{e,h}^*} \Delta + E_{c,v} \right) u_{e,h} = 1 \quad (2)$$

$$n = \int_{1/u_e}^{+\infty} N_c(E) \cdot f_n(E) dE \quad (3)$$

$$p = \int_{-\infty}^{1/u_h} N_v(E) \cdot f_p(E) dE \quad (4)$$

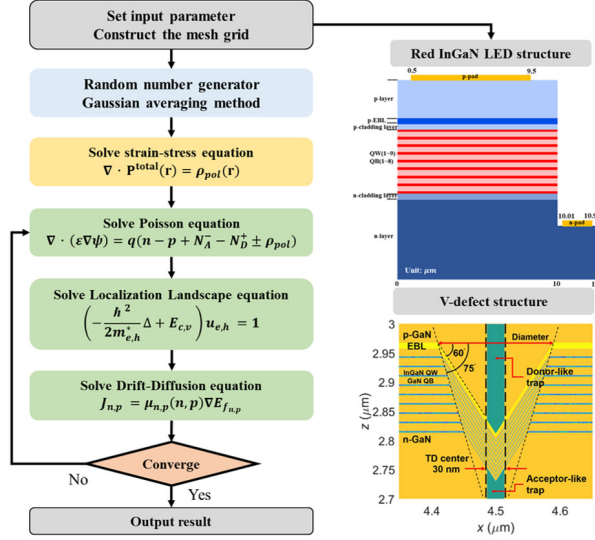


FIG. 2. Simulation flow chart of the 2D-DDCC program. The parameters of the red InGaN LED structure and the V-defect mesh setting are put in the simulation program.

To obtain the quasi-Fermi levels E_{fn} and E_{fp} , the drift-diffusion solvers [Eqs. (5) and (6)] need to be solved first.

$$J_n = -qn\mu_n\nabla E_{fn} \quad (5)$$

$$J_p = -qp\mu_p\nabla E_{fp} \quad (6)$$

where μ_n and μ_p are electron and hole mobilities, respectively. To solve the drift-diffusion equation, we need to consider the equation of continuity to make this equation into 2nd order partial different equations as shown in Eq. (7).

$$\nabla J_{n,p} = -q(R - G) \quad (7)$$

$$R = R_{SRH} + B_0np + C_0(n^2p + np^2) \quad (8)$$

$$R_{SRH} = \frac{np - n_i^2}{\tau_{n0}(p + n_i) + \tau_{p0}(n + n_i)} \quad (9)$$

Here, G is the generation rate, and R is the total recombination rate. R_{SRH} represents Shockley-Read-Hall (SRH) nonradiative recombination. n_i is the intrinsic carrier density. The carrier recombination processes, including SRH nonradiative recombination, radiative recombination, and Auger recombination, are modeled using Eqs. (8) and (9). τ_{n0} and τ_{p0} are the nonradiative lifetimes of electrons and holes, respectively. B_0 is the radiative recombination coefficient, and the electron-hole overlap in np accounts for the spatial dependence of the

carrier concentrations, i.e., $n(r)$ and $p(r)$. C_0 is the Auger recombination coefficient, where the electron-hole overlap is included in n^2p and np^2 . These recombination mechanisms are essential for determining the IQE, as shown in Eq. (10). Here, we define IQE by integrating carrier recombination in QWs and dividing it by the total injected current, which includes the charge injection efficiency η_{ie} . This definition slightly differs from the traditional one. In this paper, carrier overflow is not observed, and η_{ie} is equal to 1.0. The overall WPE, considering IQE, light extraction efficiency (LEE), and photon energy, is given in Eq. (11).

$$IQE = \frac{\int qB_0np}{\int qR} \times \eta_{ie} = \frac{\int qB_0np}{\int qR} \times \frac{\int qR}{J} = \frac{\int qB_0np}{J} \quad (10)$$

$$WPE = \frac{IQE \times LEE \times \hbar\omega}{qV} \quad (11)$$

To simulate random alloy fluctuations, we used a random number generator combined with Gaussian averaging methods to distribute indium (In) and gallium (Ga) atoms across the lattice sites within the multiple quantum wells (MQWs). This arrangement effectively simulates local compositional variations and their impact on essential metrics such as bandgap energy and polarization, ensuring accurate device characterization. Our model also accounts for the impact of tail states, which are carrier states below the bandgap that arise from crystal structure imperfections, strain-induced bandgap changes, or impurities. These tail-state effects have been widely discussed in polycrystalline, doped, or amorphous semiconductor materials. Such states provide additional carrier percolation paths, significantly influencing carrier dynamics. The origin of tail states in this paper will be discussed later. To incorporate tail states, we define the density of tail states, $N_{tail}(E)$, represented by a Gaussian distribution [Eq. (12)], as shown in Fig. 3(d). This equation describes the peak density of tail states N_{tail} , the energy center E_{tail} , and the standard deviation σ_{tail} .

$$N_{(c,v),tail}(E) = N_{tail} \exp\left(-\frac{(E - E_{tail})^2}{2\sigma_{tail}^2}\right) \quad (12)$$

When the Gaussian shape density of states allowing carriers transport in these states is considered in the Poisson drift-diffusion solver, the total density of state for carrier density is modified to

$$N_{(c,v),total}(E) = N_{(c,v)}(E) + N_{(c,v),tail}(E) \quad (13)$$

Here, $N_{(c,v),total}(E)$ replaces $N_{(c,v)}$ in Eqs. (3) and (4), allowing carriers to exist in these tail states and hop through them inside the energy bandgap, as illustrated in Fig. 3(d). Tail states have long been studied in disordered or doped semiconductors. Specifically, tail states have been identified and computed in doped GaAs, where they originate from

the local electric fields of ionized impurities³⁷. These tail-state models have been successfully implemented in our software to describe carrier transport in organic and classical semiconductors^{38–41}. Similar functions are now applied here to describe carrier transport in tail states near the TD region.

The simulation framework provides a comprehensive analysis while managing computational complexity. It is limited to a two-dimensional model with a lateral LED chip size of 10 μm . This approach captures the critical effects of tail states, V-defects, and random alloy fluctuations on $\mu\text{-LED}$ performance, offering valuable insights for the development of high-efficiency devices.

A. Parameter setting

The red InGa_N LED structure follows the design used in Ref. [8]. The structure is grown from the bottom n-GaN layer upwards, with each layer serving a specific function, as detailed in Table I. The structure begins with a 2800 nm thick n-GaN layer, which acts as the n-type contact layer and facilitates current injection. Above this, the device consists of alternating layers of n-InGa_N quantum wells (QWs) and n-GaN quantum barriers (QBs), forming the active region. The QWs, with a thickness of 2.5 nm, are designed for efficient electron-hole recombination, emitting red light. The 13.5 nm thick QBs separate each QW, enhancing carrier confinement and minimizing leakage.

Above the active region, a 10 nm p-Al_{0.15}Ga_{0.85}N electron blocking layer (EBL) is included, as in Ref. [8]. The use of an EBL is common in violet and blue LEDs to prevent electron overflow at high injection currents. However, for longer-wavelength green and red LEDs, this is generally unnecessary due to the deeper QWs, which strongly suppress carrier overflow, as well as the lower operating voltages. As long as the bias voltage remains significantly below the GaN p-n junction built-in voltage, electron overflow is negligible. Here, we retain the EBL to simulate the exact structure from Ref. [8]. The top p-GaN layer, with a thickness of 130 nm, serves as the p-type contact layer, completing the device structure.

Further material parameters, such as bandgap energies, doping concentrations, and recombination coefficients, are provided in Table I. The Auger-Meitner coefficient C_0 is chosen to be significantly larger in the InGa_N QW region, as it is well known that alloy disorder substantially increases this coefficient compared to pure GaN^{42,43}. This choice of C_0 also provides better agreement with the experimental results discussed later.

The effect of varying indium compositions in the V-defect sidewall QWs on red InGa_N LED performance was evaluated. The device structure maintains a constant indium composition of 29% in the c-plane QWs. The thin (0.67 nm) V-defect sidewall QWs were designed with an indium composition of 17%, along with 3.62 nm thick sidewall QBs. These variations lead to corresponding changes in the bandgap energies and polarization properties of the sidewall QWs, which can impact carrier dynamics and recombination efficiency. In the TD center, within 30 nm regions, there is a high density of

deep-level traps and shallow-level tail states. The deep-level trap state parameters are listed in Table II, while the tail state parameters are shown in Table III.

In this study, we include tail states in our model. The possible origins of these tail states are as follows: Near the TD center, crystal distortion occurs, significantly affecting the strain in the surrounding QW/QB regions. In red InGa_N QW LEDs, a strain variation of 2–4%, combined with deformation potentials (D_1 to D_6 ⁴⁴) ranging from 1.7 to 6.3 eV, can introduce a bandgap variation of several hundred meV. This variation may contribute to the tail states discussed here. Additionally, threading dislocations in GaN generate strong localized electric fields due to their charged nature, primarily through carrier trapping⁴⁵. These fields shift the absorption edge to lower energies, broadening the absorption tail and further leading to the presence of tail states. This effect is similar to the edge broadening observed in GaAs, as reported in Ref. [37].

Our findings indicate that tail states significantly influence carrier transport^{39,40}, particularly when strong polarization-induced fields and large band offsets hinder vertical carrier injection into the QWs, as in red LEDs. This disrupts the ideal carrier flow over barriers, as illustrated by the band structure model in Fig. 3(c). The altered energy landscape redirects carriers, increasing leakage to non-radiative pathways and promoting recombination at NR states near dislocations. Furthermore, the inclusion of tail states (Table III) modifies the density of states (DOS), as shown in Fig. 3(d). The additional energy levels introduced by tail states increase the probability of carrier trapping, enhancing nonradiative recombination in dislocation regions and reducing radiative efficiency. These effects on the DOS highlight the critical role of tail states in shaping the electronic properties and overall optical performance of the LED.

Considering the equivalent band edge densities of states (DOS) of $2.3 \times 10^{18} \text{ cm}^{-3}$ (N_c) for the conduction band and $1.8 \times 10^{19} \text{ cm}^{-3}$ (N_v) for the valence band, along with the random distribution of strain and electric fields caused by dislocations, we selected the values for tail state densities and the full width at half maximum (FWHM) of the Gaussian distribution (σ_{tail}) as presented in Table III. These values were chosen to accurately reflect typical material imperfections and their effects on carrier trapping and recombination processes. When incorporated into our simulations, these parameters closely match the experimental results for internal quantum efficiency (IQE) and current-voltage (I-V) characteristics. A comprehensive analysis of tail state formation will not be explored further in this paper.

B. Simulation models

Having defined the material parameters, we simulated four different models to separately analyze the impact of tail states, V-defects, and random alloy fluctuations on the performance of red InGa_N LEDs. The first model excluded all three factors. Figure 3(a) shows the second model, which introduces random alloy fluctuations, followed by the third model, which incorporates V-defects. Finally, the fourth model includes all

TABLE I. Parameter setting with the red InGaN LED structure.

The structure is grown from the bottom n-GaN layer upwards, with each layer having a specific role, as detailed in Table 3.1.

Material	Thickness (nm)	Bandgap (eV)	Doping (10^{18} cm^{-3})	E_a (meV)	B_0 coefficient ($10^{-11} \text{ cm}^3/\text{s}$)	C_0 coefficient ($10^{-30} \text{ cm}^6/\text{s}$)	e^-/h^+ mobility (cm^2/Vs)	$\tau_{n,p}$ (ns)
p GaN	130	3.44	30	180	3	0.2	100/5	50
p AlGaIn EBL	10	3.72	20	264	3	0.2	100/5	50
p GaN cladding layer	13.5	3.44	20	180	3	0.2	100/5	50
n GaN QB(1~8)	13.5	3.44	1	25	3	0.2	350/10	50
n InGaIn QW(7~9)	2.5	2.21	1	25	3	1.8	150/5	7
n InGaIn QW(4~6)	2.5	2.21	1	25	3	1.8	150/5	2
n InGaIn QW(1~3)	2.5	2.21	1	25	3	1.8	150/5	1.5
n GaN cladding layer	13.5	3.44	40	25	3	0.2	200/5	50
n GaN	2800	3.44	5	25	3	0.2	200/5	50

TABLE II. Parameter of trap levels located in the TD center. The energy levels of the traps (E_t are given relative and below the conduction band (E_c).

Type	Density of traps ($1/\text{cm}^3$)	τ_n, τ_p (ns)	E_t below E_c (eV)
Donor-like trap	1×10^{18}	0.5	0.6
Acceptor-like trap	1×10^{18}	0.1	3.0

TABLE III. The parameters for tail states density and FWHM of Gaussian distribution in threading dislocation lines and V-defect sidewalls. E_{tail} is zero in the setting. The value used here gives a satisfactory fit to the WPE curve shown in Ref. [8].

	Tail states density (N_{tail}) (cm^{-3})	FWHM of the Gaussian distribution (eV)
Threading dislocation line	10^{17}	0.4
V-defect sidewall QB	10^{15}	0.3

three factors: random alloy fluctuations, V-defects, and tail states, as shown in Fig. 3(b). The region containing tail states is highlighted by the yellow dashed line in the V-defect region.

III. RESULTS AND DISCUSSION

A. Carrier Injection Mechanism Through V-defects

In this section, we sequentially examine carrier injection in: (1) homogeneous semiconductor layers, (2) the presence of random alloy fluctuations, (3) the influence of V-defects, and (4) the newly added tail state leakage model. The current flow mechanisms for the four different models are analyzed at a current density of 20 A/cm^2 . Figures 4(a) and 4(b) illustrate the current flow in the first model, which does not account for random alloy fluctuations, V-defects, or defect state leakage. In this case, current is uniformly injected into the QWs, with carrier injection remaining relatively constant throughout. However, due to the absence of localized states or additional carrier transport pathways, the applied voltage must

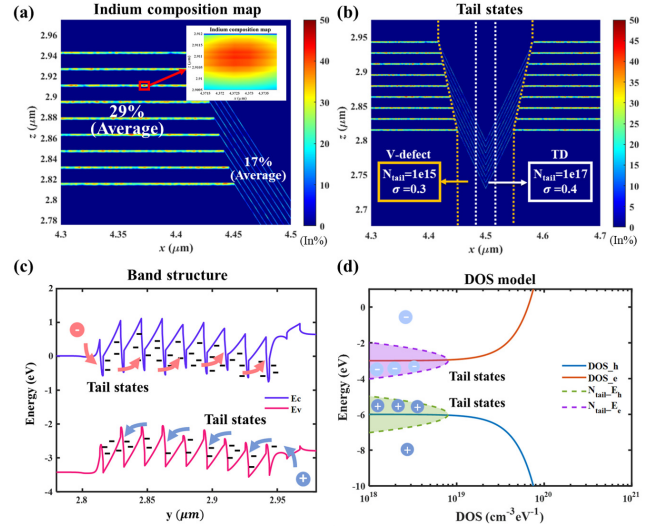


FIG. 3. Simulation models: (a) Compositional map of the combined model incorporating alloy fluctuations and V-defects. Random alloy fluctuations are illustrated in the inset. Indium composition is 17% at V-defect sidewalls QWs, averaged to 29% at c-plane MQWs, and (b) tail states along TD centers and sidewalls, acting as transport and recombination pathways, reducing the turn-on voltage and radiative efficiency, inducing a leakage current below turn-on. (c) Band structure showing carrier transport through tail states at low current density, leading to an improved carrier injection at low voltage, which is identified as carrier leakage. (d) Position of tail states in the density of states across the bandgap.

be very high (10.55V) to reach 20 A/cm^2 , indicating significantly hindered vertical carrier injection. As extensively discussed in our previous work on blue and green LEDs^{19,28,34}, the polarization-induced and band offset barriers between the QWs and QBs are even stronger in red InGaIn MQW LEDs. Consequently, the required applied voltage is much larger than in blue and green LEDs, despite the smaller QW bandgap.

In the second model, regions of increased electron and hole flow emerge due to higher local carrier concentrations in the high-indium composition regions of the QWs, introduced via random alloy fluctuations (shown in Figs. 4(c) and 4(d)). These compositional fluctuations create potential variations,

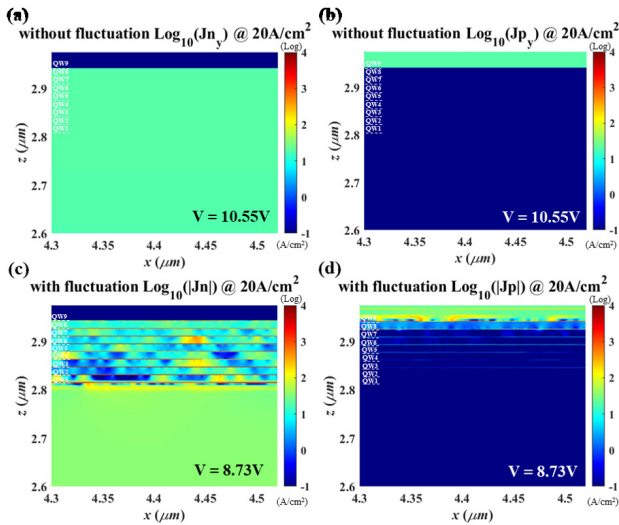


FIG. 4. The (a, c) electron and (b, d) hole current density distribution of the first two models at current density 20 A/cm^2 . In (a) and (b), the applied voltage is $V = 10.55 \text{ V}$, while in (c) and (d), the applied voltage is $V = 8.73 \text{ V}$. Fluctuations create fluctuated current flowing paths and higher local carrier concentrations, which may lead to locally enhanced recombination in the higher indium sites.

enabling current flow through lower-barrier sites while also providing localized carrier confinement. Compared to the previous model, the applied voltage ($\sim 8.73 \text{ V}$) at 20 A/cm^2 is lower than in the uniform composition case, indicating that fluctuations help reduce energy barriers for carrier injection. Nonetheless, the applied voltage remains significantly high, failing to explain or replicate the low operating voltages observed in InGaN red LEDs. When carriers encounter low-energy barrier sites, they preferentially inject through these regions and subsequently diffuse laterally, as illustrated in Fig. 4(d).

In Fig. 5(a-b), V-defects and random alloy fluctuations are incorporated into the third model. Since the sidewalls of the QWs are semipolar planes with minimal piezoelectric polarization, the V-defects provide an additional channel for carrier injection. As a result, carrier flow into the c-plane QWs is more efficient through the sidewalls of the V-defects. The reduced barriers, caused by the lower piezoelectric polarization, allow for a more concentrated current density at the V-defect sites, where the voltage at a current density of 20 A/cm^2 significantly drops to 2.85 V . Additionally, carriers trapped along the TD lines may lead to nonradiative recombination losses. Although the forward voltage decreases significantly, it remains higher than the experimental value of approximately 2.1 V at 1 A/cm^2 . This discrepancy arises because, although the V-defect $\{10\bar{1}1\}$ semipolar plane ($\sim 62^\circ$) exhibits nearly zero polarization at the interface, it typically features a thinner QW with a lower indium composition, similar to that of blue/violet MQWs. The theoretical turn-on voltage of blue LEDs is approximately 2.72 V ($\hbar\omega = 2.72 \text{ eV}$). Consequently, the sidewall QW aids carrier injection once it becomes conductive. Even if the sidewall QW had a higher indium com-

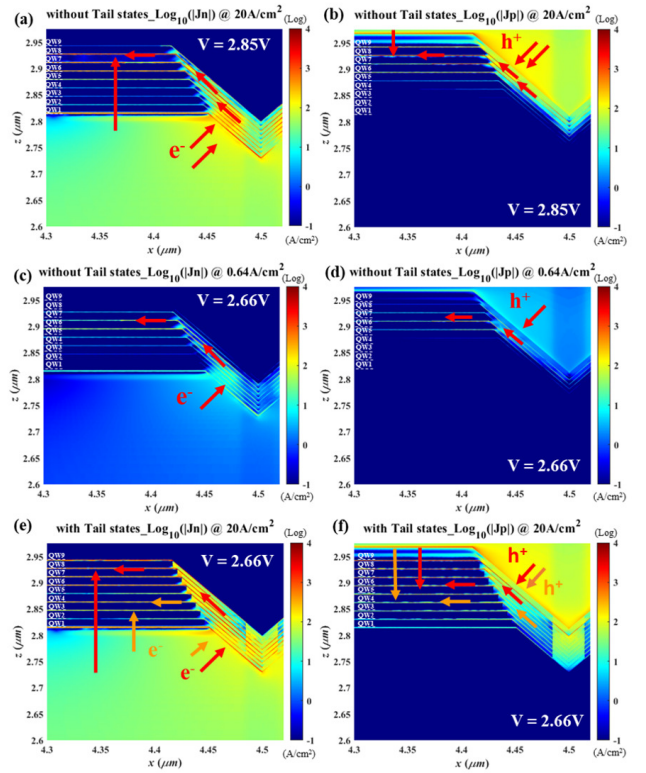


FIG. 5. Computations of current density distributions of (a, c, e) electrons and (b, d, f) holes at applied voltages of $V = 2.85 \text{ V}$ and 2.66 V for the third model (compositional fluctuations + V-defects, (a, c) and (b, d), and for the fourth model (addition of tail states (e, f)). V-defects improve carrier flow while tail states increase leakage and nonradiative recombination in the defect region. However, holes are then leaking to lower QWs so that more QWs will emit light. Also, a lower V_{for} is needed to reach a current density of 20 A/cm^2 compared to the model without tail states.

position (22%) instead of the 17% used, the voltage would decrease slightly but still would not reach the low turn-on voltage due to the increased band offset in the QW and the higher series resistance resulting from the presence of nine deeper sidewall QWs. Therefore, incorporating a tail state current transport model is necessary.

The interplay between V-defects, random alloy fluctuations, and tail states plays a crucial role in carrier dynamics and device performance. Localized low-energy zones at the TD centers significantly enhance carrier injection, as shown by the conduction and valence band distributions in Fig. 6. Electrons trapped by deep-level states in the n-layer induce a potential barrier at the TD center, while trapped holes in the p-type layer also create a potential barrier in the TD center. In the active region of the TD, electrons and holes recombine non-radiatively. Furthermore, if tail states are considered, their high density near the TD region may lead to increased local carrier concentrations and currents.

When the voltage is lowered to 2.66 V , fewer carriers are injected in the third model due to the absence of defect-mediated pathways, requiring a higher voltage to achieve compara-

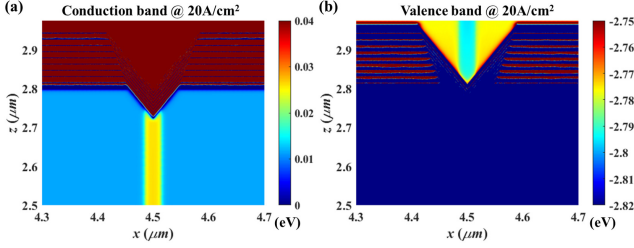


FIG. 6. The plot of (a) conduction band potential and (b) valence band potential distributions at 20 A/cm^2 with a selected scale range to show the potential barrier induced by electron and hole-trapped charges in the TD center (traps parameters in table II).

ble injection levels (Fig. 5(c, d)). However, in the fourth model, which includes tail states, the current density reaches 20 A/cm^2 at this voltage (Fig. 5(e, f)). These tail states are incorporated into the V-defect region in the fourth model, with N_{tail} being higher at the defect center (the location of the dislocation line, Fig. 3(b)). The higher current densities in the TD area (Figs. 5(c) and 5(f)) indicate that these tail states increase the current, particularly at lower voltages, while also leading to greater nonradiative recombination, as the TD area contains fast nonradiative recombination traps. The tail states also create leakage paths toward nonradiative centers, reducing overall efficiency. However, they facilitate carrier injection into the QWs at low voltages, as some leakage current diffuses into the QWs. Once carriers begin injecting into the c-plane quantum well (QW), they screen the polarization field, particularly at the corners of the c-plane/semipolar plane interface. This screening effect reduces the injection barrier in the c-plane region. Comparing Figs. 5(d) and 5(f) for hole injection at the same voltage, we observe slightly stronger vertical injection in the c-plane or semipolar plane, especially at the QW corners. Additionally, the J-V curves in Figs. 7 and 8 indicate that this change is not limited to leakage current below the turn-on voltage: the entire J-V curve shifts to a lower voltage.

To further analyze these effects, the current density-voltage (J-V) characteristics were evaluated for the four models, as shown in Fig. 7(a). The forward voltage V_{for} decreases as more mechanisms are incorporated, indicating improved carrier injection efficiency. Random alloy fluctuations alone lead to a noticeable reduction in V_{for} by smoothing potential barriers, while the addition of V-defects further enhances injection efficiency by introducing additional low-energy pathways through the sidewall QWs. Tail states, however, have a more complex impact, as shown in the log-scale IV curve (Fig. 7(b)). While they assist carrier injection at lower voltages by providing leakage paths, they also increase nonradiative recombination, particularly in the TD regions. Overall, the V-defect and additional tail state models help reduce the operating voltage but decrease the IQE when these defects are present. The influence of tail states can be further examined in the log(J)-V curve, as shown in Fig. 8(a). Many experimental studies⁴⁶⁻⁵⁰ report significant leakage current for voltages smaller than $\frac{\hbar\omega}{q}$. For example, Ref. [29] reports a sub turn-on

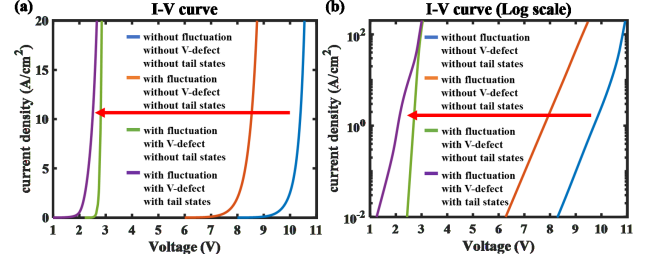


FIG. 7. (a) The IV curves show the decrease of turn-on voltage as more mechanisms are included, indicating improved carrier injection efficiency. (b) The log-scale IV curve shows the leakage current caused by tail states, indicating how these states contribute to increased carrier leakage under forward bias.

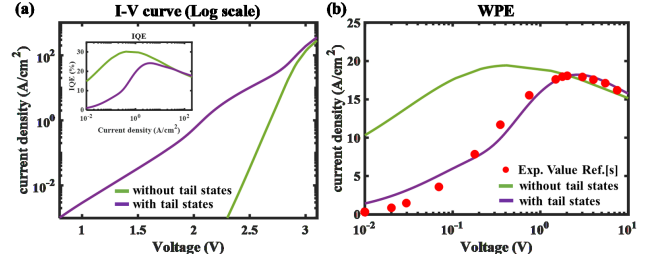


FIG. 8. (a) Expanded Log(I)-V plot of with/without the tail states leakage model. The tail states-model can explain the leakage behavior of the LED structure. It also enhances current injection into QWs at $V < 2.6\text{V}$. (b) Plot of WPE as a function of current with or without tail states. Tail states decrease WPE at low voltage as injection occurs in the TD region, with trapping by nonradiative recombination centers at dislocations. At increased voltage, injection occurs in the QW regions, thus almost recovering the original WPE without tail states. Overall, the peak WPE penalty is quite limited. The experimental value (Ref.[8]) is from the Ref.[8].

voltage slope of approximately 393 mV/dec below the turn-on voltage. This low-voltage current behavior can be well represented by implementing the tail state model, as shown in Fig. 8(a), by choosing appropriate values for N_{tail} and σ_{tail} in Eqn. (12). While growing epitaxial layers with more defects can reduce the operating voltage, it also increases nonradiative losses. Hence, a balance must be struck between IQE and voltage to optimize WPE.

The WPE curve in Fig. 8(b), assuming 85% light extraction efficiency, shows that at low voltage, WPE is significantly reduced as most carrier injection occurs in the region with tail states, i.e., the TD region. However, at higher voltages, due to the screening effect in the QWs caused by leakage carriers, injection shifts to regions farther from the TD, almost recovering the WPE value observed without tail states.

IV. CONCLUSION

In this study, the effects of V-defects, random alloy fluctuations, and tail states were simultaneously considered to understand carrier injection and the low turn-on voltage perfor-

mance of red InGaN LEDs. The inclusion of leakage currents and nonradiative recombination losses greatly improved the agreement between simulation results and experimental data compared to models considering only alloy disorder and V-defects. The tail state model not only explained the low forward voltage but also provided insight into enhanced nonradiative recombination in low-current-density regions. However, the penalty in peak WPE was found to be minimal. The random alloy, V-defect, and tail state models together help elucidate the physics of LED devices and may guide efforts to improve red InGaN LED performance by optimizing the balance between defect densities and carrier transport mechanisms to maximize both IQE and turn-on voltage, and thus WPE. These findings should provide a valuable foundation for future advancements in high-efficiency LED applications and designs.

ACKNOWLEDGMENTS

This project is supported by National Science and Technology Council (NSTC) under grant No. 112-2221-E-002-215-MY3, 113-2640-E-002-005, and 113-2124-M-002-013-MY3. Support at UCSB was provided by the Solid State Lighting and Energy Electronics Center (SSLEEC); U.S. Department of Energy under the Office of Energy Efficiency & Renewable Energy (EERE) Award No. DE-EE0009691; the National Science Foundation (NSF) RAISE program (Grant No. DMS-1839077); the Simons Foundation (Grant #s 601952 and 1027114 for JSS and CW, respectively).

AUTHOR DECLARATIONS

Huai-Chin Huang: conceptualization (equal); data curation (lead); formal analysis (equal); methodology (support); validation (lead); visualization(lead); writing – original draft (lead).

Shih-Min Chen: conceptualization (support); data curation (support); formal analysis (equal); validation (support).

Claude Weisbuch: conceptualization (equal);writing-review and editing (equal). supervision (support)

James S. Speck: conceptualization (equal);writing-review and editing (equal). funding acquisition (equal); supervision (support);

Yuh-Renn Wu conceptualization (equal); formal analysis (equal); funding acquisition (lead); project administration (lead); software(lead); supervision (lead); writing-review and editing (lead).

CONFLICT OF INTEREST

The authors have no conflicts to disclose

DATA AVAILABILITY STATEMENT

The data that support the findings of this study are available from the corresponding author upon reasonable request.

V. REFERENCES

- ¹J. Day, J. Li, D. Lie, C. Bradford, J. Lin, and H. Jiang, “III-Nitride full-scale high-resolution microdisplays,” *Applied Physics Letters* **99**, 031116 (2011).
- ²J. Lin and H. Jiang, “Development of microled,” *Applied Physics Letters* **116**, 100502 (2020).
- ³A. Pandey and Z. Mi, “III-nitride nanostructures for high efficiency micro-LEDs and ultraviolet optoelectronics,” *IEEE Journal of Quantum Electronics* **58**, 1–13 (2022).
- ⁴C.-C. Lin, Y.-R. Wu, H.-C. Kuo, M. S. Wong, S. P. DenBaars, S. Nakamura, A. Pandey, Z. Mi, P. Tian, K. Ohkawa, *et al.*, “The micro-LED roadmap: status quo and prospects,” *Journal of Physics: Photonics* **5**, 042502 (2023).
- ⁵C. Weisbuch, “On the search for efficient solid state light emitters: Past, present, future,” *ECS Journal of Solid State Science and Technology* **9**, 016022 (2019).
- ⁶C.-H. Ho, J. S. Speck, C. Weisbuch, and Y.-R. Wu, “Efficiency and forward voltage of blue and green lateral LEDs with V-shaped defects and random alloy fluctuation in quantum wells,” *Physical Review Applied* **17**, 014033 (2022).
- ⁷F.-P. Massabuau, M. J. Davies, F. Oehler, S. Pamerter, E. Thrush, M. J. Kappers, A. Kovacs, T. Williams, M. A. Hopkins, C. J. Humphreys, *et al.*, “The impact of trench defects in InGaN/GaN light emitting diodes and implications for the “green gap” problem,” *Applied Physics Letters* **105**, 112110 (2014).
- ⁸S. Zhang, J. Zhang, J. Gao, X. Wang, C. Zheng, M. Zhang, X. Wu, L. Xu, J. Ding, Z. Quan, *et al.*, “Efficient emission of InGaN-based light-emitting diodes: toward orange and red,” *Photonics Research* **8**, 1671–1675 (2020).
- ⁹D. Nath, Z. Yang, C.-Y. Lee, P. Park, Y.-R. Wu, and S. Rajan, “Unipolar vertical transport in GaN/AlGaIn/GaN heterostructures,” *Applied Physics Letters* **103**, 022102 (2013).
- ¹⁰G. Lheureux, C. Lynsky, Y.-R. Wu, J. S. Speck, and C. Weisbuch, “A 3D simulation comparison of carrier transport in green and blue c-plane multi-quantum well nitride light emitting diodes,” *Journal of Applied Physics* **128**, 235703 (2020).
- ¹¹C. Lynsky, A. I. Alhassan, G. Lheureux, B. Bonef, S. P. DenBaars, S. Nakamura, Y.-R. Wu, C. Weisbuch, and J. S. Speck, “Barriers to carrier transport in multiple quantum well nitride-based c-plane green light emitting diodes,” *Physical Review Materials* **4**, 054604 (2020).
- ¹²K. Qwah, M. Monavarian, G. Lheureux, J. Wang, Y.-R. Wu, and J. Speck, “Theoretical and experimental investigations of vertical hole transport through unipolar AlGaIn structures: Impacts of random alloy disorder,” *Applied Physics Letters* **117**, 022107 (2020).
- ¹³X. Wu, C. Elsass, A. Abare, M. Mack, S. Keller, P. Petroff, S. DenBaars, J. Speck, and S. Rosner, “Structural origin of V-defects and correlation with localized excitonic centers in InGaIn/GaN multiple quantum wells,” *Applied Physics Letters* **72**, 692–694 (1998).
- ¹⁴T.-J. Yang, R. Shivaraman, J. S. Speck, and Y.-R. Wu, “The influence of random indium alloy fluctuations in indium gallium nitride quantum wells on the device behavior,” *Journal of Applied Physics* **116**, 113104 (2014).
- ¹⁵S. Nakamura, “The roles of structural imperfections in InGaIn-based blue light-emitting diodes and laser diodes,” *Science* **281**, 956–961 (1998).
- ¹⁶B. Heying, E. Tarsa, C. Elsass, P. Fini, S. DenBaars, and J. Speck, “Dislocation mediated surface morphology of GaN,” *Journal of Applied Physics* **85**, 6470–6476 (1999).
- ¹⁷A. N. Bright, N. Sharma, and C. J. Humphreys, “Analysis of contacts and v-defects in GaN device structures by transmission electron microscopy,” *Microscopy* **50**, 489–495 (2001).
- ¹⁸L. Le, D. Zhao, D. Jiang, L. Li, L. Wu, P. Chen, Z. Liu, J. Yang, X. Li, X. He, *et al.*, “Effect of V-defects on the performance deterioration of In-GaN/GaN multiple-quantum-well light-emitting diodes with varying barrier layer thickness,” *Journal of Applied Physics* **114**, 143706 (2013).

- ¹⁹J. Kim, Y.-H. Cho, D.-S. Ko, X.-S. Li, J.-Y. Won, E. Lee, S.-H. Park, J.-Y. Kim, and S. Kim, "Influence of v-pits on the efficiency droop in InGaN/GaN quantum wells," *Optics express* **22**, A857–A866 (2014).
- ²⁰H. Wang, X. Wang, Q. Tan, and X. Zeng, "V-defects formation and optical properties of InGaN/GaN multiple quantum well LED grown on patterned sapphire substrate," *Materials Science in Semiconductor Processing* **29**, 112–116 (2015).
- ²¹Q. Nie, Z. Jiang, Z. Gan, S. Liu, H. Yan, and H. Fang, "Defect analysis of the LED structure deposited on the sapphire substrate," *Journal of Crystal Growth* **488**, 1–7 (2018).
- ²²R. Yapparov, Y. C. Chow, C. Lynsky, F. Wu, S. Nakamura, J. S. Speck, and S. Marcinkevičius, "Variations of light emission and carrier dynamics around V-defects in InGaN quantum wells," *Journal of Applied Physics* **128**, 225703 (2020).
- ²³A. B. M. H. Islam, T. K. Kim, D.-S. Shin, J.-I. Shim, and J. S. Kwak, "Generation of sidewall defects in InGaN/GaN blue micro-LEDs under forward-current stress," *Applied Physics Letters* **121**, 013501 (2022).
- ²⁴F. Wu, J. Ewing, C. Lynsky, M. Iza, S. Nakamura, S. P. DenBaars, and J. S. Speck, "Structure of V-defects in long wavelength GaN-based light emitting diodes," *Journal of Applied Physics* **133**, 035703 (2023).
- ²⁵S. Marcinkevičius, T. Tak, Y. C. Chow, F. Wu, R. Yapparov, S. P. DenBaars, S. Nakamura, and J. S. Speck, "Dynamics of carrier injection through V-defects in long wavelength GaN LEDs," *Applied Physics Letters* **124**, 181108 (2024).
- ²⁶S.-H. Han, D.-Y. Lee, H.-W. Shim, J. Wook Lee, D.-J. Kim, S. Yoon, Y. Sun Kim, and S.-T. Kim, "Improvement of efficiency and electrical properties using intentionally formed V-shaped pits in InGaN/GaN multiple quantum well light-emitting diodes," *Applied Physics Letters* **102**, 251123 (2013).
- ²⁷C.-K. Li, C.-K. Wu, C.-C. Hsu, L.-S. Lu, H. Li, T.-C. Lu, and Y.-R. Wu, "3D numerical modeling of the carrier transport and radiative efficiency for InGaN/GaN light emitting diodes with V-shaped pits," *AIP Advances* **6**, 055208 (2016).
- ²⁸C.-K. Li, M. Piccardo, L.-S. Lu, S. Mayboroda, L. Martinelli, J. Peretti, J. S. Speck, C. Weisbuch, M. Filoche, and Y.-R. Wu, "Localization landscape theory of disorder in semiconductors. III. application to carrier transport and recombination in light emitting diodes," *Physical Review B* **95**, 144206 (2017).
- ²⁹F.-H. Hsiao, T.-Y. Lee, W.-C. Miao, Y.-H. Pai, D. Iida, C.-L. Lin, F.-C. Chen, C.-W. Chow, C.-C. Lin, R.-H. Horng, *et al.*, "Investigations on the high performance of InGaN red micro-LEDs with single quantum well for visible light communication applications," *Discover Nano* **18**, 95 (2023).
- ³⁰J. Park, E.-J. Youn, W. J. Baek, E.-K. Chu, H. S. Kim, D.-M. Geum, J. P. Kim, B. H. Kim, S.-H. Kuk, H.-H. Park, *et al.*, "Size-dependent optoelectronic characteristics of InGaN/GaN red micro-LEDs on 4-inch si substrates: high pixel density arrays demonstration," *Optics Express* **32**, 24242–24250 (2024).
- ³¹H.-T. Shen, C. Weisbuch, J. S. Speck, and Y.-R. Wu, "Three-dimensional modeling of minority-carrier lateral diffusion length including random alloy fluctuations in (In, Ga) N and (Al, Ga) N single quantum wells," *Physical Review Applied* **16**, 024054 (2021).
- ³²M. A. Der Maur, D. Baretin, A. Pecchia, F. Sacconi, and A. Di Carlo, "Effect of alloy fluctuations in InGaN/GaN quantum wells on optical emission strength," in *Numerical Simulation of Optoelectronic Devices, 2014* (IEEE, 2014) pp. 11–12.
- ³³C. Robertson, K. Qwah, Y.-R. Wu, and J. Speck, "Modeling dislocation-related leakage currents in GaN pn diodes," *Journal of Applied Physics* **126**, 245705 (2019).
- ³⁴Y.-R. Wu, R. Shivaraman, K.-C. Wang, and J. S. Speck, "Analyzing the physical properties of InGaN multiple quantum well light emitting diodes from nano scale structure," *Applied Physics Letters* **101**, 083505 (2012).
- ³⁵M. Filoche, M. Piccardo, Y.-R. Wu, C.-K. Li, C. Weisbuch, and S. Mayboroda, "Localization landscape theory of disorder in semiconductors. I. theory and modeling," *Physical Review B* **95**, 144204 (2017).
- ³⁶M. Piccardo, C.-K. Li, Y.-R. Wu, J. S. Speck, B. Bonef, R. M. Farrell, M. Filoche, L. Martinelli, J. Peretti, and C. Weisbuch, "Localization landscape theory of disorder in semiconductors. II. Urbach tails of disordered quantum well layers," *Physical Review B* **95**, 144205 (2017).
- ³⁷H. Casey Jr and F. Stern, "Concentration-dependent absorption and spontaneous emission of heavily doped GaAs," *Journal of Applied Physics* **47**, 631–643 (1976).
- ³⁸T. Kirchartz, B. E. Pieters, J. Kirkpatrick, U. Rau, and J. Nelson, "Recombination via tail states in polythiophene: fullerene solar cells," *Physical Review B—Condensed Matter and Materials Physics* **83**, 115209 (2011).
- ³⁹T.-J. Kung, J.-Y. Huang, J.-J. Huang, S. H. Tseng, M.-K. Leung, T.-L. Chiu, J.-H. Lee, and Y.-R. Wu, "Modeling of carrier transport in organic light emitting diode with random dopant effects by two-dimensional simulation," *Optics Express* **25**, 25492–25503 (2017).
- ⁴⁰J.-Y. Huang, J.-H. Lee, Y.-R. Wu, T.-Y. Chen, Y.-C. Chiu, J.-J. Huang, M.-k. Leung, and T.-L. Chiu, "Revealing the mechanism of carrier transport in host-guest systems of organic materials with a modified poisson and drift-diffusion solver," *Physical Review Materials* **4**, 125602 (2020).
- ⁴¹J.-Y. Huang, H.-C. Hung, K.-C. Hsu, C.-H. Chen, P.-H. Lee, H.-Y. Lin, B.-Y. Lin, M.-k. Leung, T.-L. Chiu, J.-H. Lee, *et al.*, "Numerical analysis and optimization of a hybrid layer structure for triplet–triplet fusion mechanism in organic light-emitting diodes," *Advanced Theory and Simulations* **6**, 2200633 (2023).
- ⁴²M. Shahmohammadi, W. Liu, G. Rossbach, L. Lahourcade, A. Dussaigne, C. Bougerol, R. Butté, N. Grandjean, B. Deveaud, and G. Jacopin, "Enhancement of Auger recombination induced by carrier localization in InGaN/GaN quantum wells," *Physical Review B* **95**, 125314 (2017).
- ⁴³H.-Y. Ryu, G.-H. Ryu, C. Onwukaeme, and B. Ma, "Temperature dependence of the Auger recombination coefficient in InGaN/GaN multiple-quantum-well light-emitting diodes," *Optics Express* **28**, 27459–27472 (2020).
- ⁴⁴H.-H. Huang and Y.-R. Wu, "Study of polarization properties of light emitted from a-plane InGaN/GaN quantum well-based light emitting diodes," *Journal of Applied Physics* **106**, 023106 (2009).
- ⁴⁵H. Hasegawa, Y. Kamimura, K. Edagawa, and I. Yonenaga, "Dislocation-related optical absorption in plastically deformed GaN," *Journal of Applied Physics* **102**, 026103 (2007).
- ⁴⁶M. S. Wong, C. Lee, D. J. Myers, D. Hwang, J. A. Kearns, T. Li, J. S. Speck, S. Nakamura, and S. P. DenBaars, "Size-independent peak efficiency of III-nitride micro-light-emitting-diodes using chemical treatment and sidewall passivation," *Applied Physics Express* **12**, 097004 (2019).
- ⁴⁷Z. Zhuang, D. Iida, and K. Ohkawa, "Effects of size on the electrical and optical properties of InGaN-based red light-emitting diodes," *Applied Physics Letters* **116**, 173501 (2020).
- ⁴⁸Z. Zhuang, D. Iida, and K. Ohkawa, "Investigation of InGaN-based red/green micro-light-emitting diodes," *Optics Letters* **46**, 1912–1915 (2021).
- ⁴⁹X. Liu, Y. Sun, Y. Malhotra, A. Pandey, P. Wang, Y. Wu, K. Sun, and Z. Mi, "N-polar InGaN nanowires: breaking the efficiency bottleneck of nano and micro LEDs," *Photonics Research* **10**, 587–593 (2022).
- ⁵⁰A. Pandey, M. Reddeppa, and Z. Mi, "Recent progress on micro-LEDs," *Light: Advanced Manufacturing* **4**, 519–542 (2024).